Regional wise characteristic study of significant wave height for the Indian Ocean

S. Sreelakshmi[1] · Prasad K. Bhaskaran[1]

Abstract

A proper knowledge and understanding of wind-wave characteristics and its variability on basin, regional and local scales have profound importance and practical applications in marine related activities, ocean engineering, and coastal zone management. The present study deals with the comparison of synoptic annual trends derived from space borne measurements (1992–2016), ERA-5 (1992–2018), and NCEP WWIII global run (1997–2018), monthly and seasonal wave climatology, characteristics of the annual cycle in regional basins and monthly trends of wind-wave climate on a pentad scale. Evaluation of wind-wave characteristics was performed for sub-divided domains of the IO. Further, the wave heights were segregated into percentile ranks (from 99th to 10th) by which a detailed analysis was carried out at the regional scale. Analysis of monthly and seasonal climatology signifies that the highest wave activity is observed in the extra tropical South Indian Ocean (ETSI) and the least in the Bay of Bengal. Higher percentile waves (99th, 95th, and 90th) in the ETSI are observed to be active for more than 6 months in a year. In the Arabian Sea, the maximum occurrence of 99th percentile waves (about 65%) is prominent during the month of July. An apparent pentad variation has been identified in the ETSI from 1997 to 2016 whereas, decadal variability in the north Indian Ocean (NIO) and Tropical South Indian Ocean for the lower percentile significant wave heights (25th and 10th percentiles). During the period 2007–2011, the IO experienced a considerable decreasing wave activity in all the sectors. The observed trends in annual maximum significant wave height for the ETSI and the annual mean significant wave height for the NIO are found increasing at a rate of 3.3 cm/year and 0.27 cm/year, respectively.

Keywords Indian Ocean · Significant wave height · Satellite-altimetry · Pentad-scale variability

1 Introduction

The wind-wave climate for any given region is characterized by the blended effect resulting from mutual interaction between two or more concurrent wave systems, which carry the local and remotely generated information of winds (Pomaro et al. 2018). IPCC-AR5 (Intergovernmental Panel on Climate Change-Fifth Assessment Report) highlighted on the importance of wind-waves as they play an active role in the exchange of momentum across the air–sea interface. The wind-waves have profound impact on coastal hydrodynamics, navigation, recreation, marine operations, ocean and coastal engineering activities etc. The accurate representation of wind-wave climatology is indeed required as input in many applications such as soft and hard measures for coastal protection, marine exploitation, ship routing, marine weather forecasting, etc. Therefore, it is very important to understand the basin scale trend of wind-waves during the period in which a substantial wave record is available. The wind-wave information can be acquired from observational and model products where the latter is in turn strongly dependent on the quality of forcing wind fields, basic model physics, and inherent parameterization schemes (Komen et al. 1994).

The data for wind-wave climate study requires substantial temporal and spatial coverage and can be obtained from various sources such as in situ observations, model products or space-borne measurements. The wind-wave climate study based on real-time in situ data especially for the IO is relatively small in number and sparsely distributed (Bhaskaran 2019). However, the observational data retrieved from buoy and voluntary observing ships (VOS) are now globally

✉ Prasad K. Bhaskaran
  prasadlsu@yahoo.com; pkbhaskaran@naval.iitkgp.ernet.in

1   Department of Ocean Engineering and Naval Architecture,
    Indian Institute of Technology Kharagpur, Kharagpur,
    West Bengal 721 302, India

accepted and observed to be highly beneficial for location specific studies. The major advantages of satellite data over the conventional in situ methods are its global coverage over a longer period, and that finds interesting applications in the domain of wind-wave climate study. About ten altimeter missions starting from ERS-1 to SARAL-Altika were operated over the last 28 years, providing continuous space-borne measurement of global significant wave height (H_S). Nevertheless, the satellite data finds importance and can be utilized for global, regional, as well location specific studies, and preferably, data analyzed are from the same platform (Vinoth and Young 2011). A pioneering study by Queffeulou (2003, 2004) addressed the limitation of uniformity in datasets obtained from various altimeters and proposed necessary bias correction for research purpose. A merged, calibrated altimeter wave height-database are available with daily data files in a standard format from the URL link ftp://ifremer.fr/ifremer/cersat/products/swath/altimeters/waves/. The merged calibrated space-borne data is highly recommended for climate analyses and being used for the validation of modelled, reanalysis and ensemble products and one can find out more aspects in the following studies, Aboobacker et al. (2011), Gupta et al. (2015, 2017) and Patra and Bhaskaran (2016, 2017).

The wave models are indeed important in routine hindcast and forecast of ocean waves, and the third generation wave models such as WAM (Komen et al. 1994), and WAVE-WATCH III (Tolman 1991, 2009) are widely used in regional and global scale investigations (Alves 2006; Amrutha et al. 2016; Remya et al. 2016; Swain et al. 2019). The WW III global ocean model was developed at NCEP (National Centers for Environmental Prediction)/NOAA (National Oceanic and Atmospheric Administration) inspired from WAM model. Bhaskaran (2019) reviewed the recent developments in the numerical and computation techniques and addressed the future direction of ocean wave modelling perspectives highlighting on better physical parameterization and role of high-performance computational facilities.

The European Centre for Medium-Range Weather Forecasts (ECMWF's) has been contributing the global reanalysis datasets since 1989. ERA-interim data, which is the successor of ERA-40, was well recognized and accepted through several global, regional, and location-specific studies, and the following are a few of them conducted in the IO regime (Shanas and Sanil Kumar 2014a, b; Anoop et al. 2015; Kumar and Naseef 2015; Shanas and Kumar 2015). ERA5 is the fifth generation climate reanalysis dataset produced with substantial amendments to the ERA-interim reanalysis data (Hersbach and Dick 2016; Hoffmann et al. 2019). ERA5 is provided specifically with a higher spatial and temporal resolution and is currently available from 1979 using 4D data assimilation. A study by Muhammed Naseef and Sanil Kumar (2019) validated the ERA5 surface waves

with in situ observations from 4 buoy locations and found the ERA5 annual mean H_S is close to that of deep water buoys in the Arabian Sea (AS, bias of -0.07) and the Bay of Bengal (BoB, bias of $+0.18$ m). At the same time, their study revealed an underestimation of annual average H_S and annual maximum H_S at near coast buoy location of the AS.

There are relevant studies on wave climatology both for the global and regional scales (Alves 2006; Young et al. 2011; Young and Ribal 2019; Cavaleri 2000; Cavaleri and Bertotti 2004; Cavaleri et al. 2010). A study on the global wind-wave climate by (Semedo et al. 2011) advocates the existence of a strong wind-wave climate for the Indian sector in the Southern Ocean and, highlighted the importance of the highest seasonal mean wave height. A study by Zheng et al. (2016a) using 44 years of ERA-40 wave data reported the decadal-scale variability in global oceans and pointed out the significance of regional differences and the small-scale temporal variabilities observed to be co-existing. Thus, the relative trend of wave climate observed from the global studies has necessitated the importance of regional research in the IO.

Moreover, recent few studies addressed the impact and role of climate indices that attributes to the Indian met-ocean dynamics. Kumar et al. (2016) examined the climate indices viz: El Niño–Southern Oscillation (ENSO), Indian Ocean Dipole (IOD), and Southern Annular Mode (SAM) for the IO using ERA-20C reanalysis data for 54 years. Kumar et al. (2019) investigated the influence of natural climate variability on winds and extreme ocean surface wave heights in the Indian Ocean. Their study analyzed seasonal extreme significant wave height and winds in the IO using ERA-20C reanalysis data covering the period 1957–2010. The nonstationary generalized extreme value distribution was used to understand the climate extremes considering the climate indices as covariates. Significant findings from their study (Kumar et al. 2019) indicates an increasing wave trend in the BoB, southwest tropical Indian Ocean, Southern Indian Ocean, and the South China Sea (SCS), which is possibly anticipated by the influence of ENSO and postulated on the compounding effects induced by the climate indices on the extreme H_S. In contrast, they noticed a decreased activity in the Arabian Sea (AS). A study by Arora and Dash (2019) concerned to the NIO, hypothesized that the Indian Ocean Dipole (IOD) plays an inter-connecting link between El Niño Modoki and the Tropical Cyclone Potential Intensity (TCPI) in the NIO. These studies further indicate that the analyses on the wind-wave variability and the role of remote forcing effects in controlling its variability indeed require more attention.

It is evident from the previous studies that the variability of atmospheric and oceanic parameters is sensitive to the spatial domain as well the time span under consideration. For example, a study using satellite altimeter H_S

and wind speed data (Kumar et al. 2013) has signified the higher variability of wind speed in the south Indian Ocean (SIO). Similarly, for SIO, Bhaskaran et al. (2014) and Gupta et al. (2015) highlighted that the SO storm belt had experienced the largest variability based on a comprehensive analysis of altimeter wind and wave data for a period of 21 years (1992–2012). The central Bay of Bengal (Shanas and Sanil Kumar 2014b) showed a declining trend in high wave activity during the SW monsoon. In a recent study conducted for IO using ERA5 data, Muhammed Naseef and Sanil Kumar (2019) reported an apparent decrease in H_S over major areas of IO during the period 1991–2017, the analysis based on satellite observations assimilated with ECMWF products, whereas an increase in H_S was reported when a time window of 1979–2017 was considered. Therefore, it is also crucial to introspect on the variability of wind-waves at various sectors of the IO for smaller time scales. The present study intends to establish the characteristics and variability of waves in IO from a climatological aspect in short-term time scales.

There are few studies conducted on wind-wave climate variability in the IO. These studies analyzed datasets from space-borne measurements, reanalyzed model products and few in situ observations (Gowthaman et al. 2013; Shanas and Sanil Kumar 2014a, b; Gupta et al. 2015; Amrutha et al. 2016). In a broader perspective, the outcome from previous studies provided knowledge on the basin scale characteristics and variability of wind-waves in a changing climate scenario for the IO. In-situ observations such as wave rider buoys provide only location specific data on the wind-wave climate. However, a comprehensive assessment and evaluation of wind-wave climate and its variability at different geographical locations using datasets from multiple platforms for the IO was also missing in the previous studies. In addition, a comprehensive analysis of extreme wind-waves based on percentile ranks over different identified regions in IO is the novelty of the present study. Identifying these gaps, the present study is an attempt to understand the characteristics and variability of significant wave height in IO using datasets of multiple platforms that was critically examined at regional scales.

Since there are different spatially distributed datasets, which can be obtained from the space borne, model, and reanalysis outputs, this study put effort to compare the ocean waves using altimeter, ERA5, and WWIII derived significant wave heights. This study specifically focuses on a comprehensive analysis of satellite altimetry data (~ 26 years) obtained for the IO, to understand the H_S variability in the identified sub-domains. To accomplish this objective, spatially gridded monthly-averaged dataset was used after post-processing the daily swath data files, which are quality checked and validated.

2 Study area

The Indian Ocean wave climate has been a topic of immense interest in a changing climate scenario to the scientific community attributed primarily due to its geographical setting and the reversing monsoon system. The IO is connected with the Southern Ocean along the southern boundary and with the Pacific Ocean exchanging water mass through the Indonesian Through-flow and the Tasman leakage (van Sebille et al. 2014). The two semi-marginal seas, namely the AS and BoB along the west and east of the Indian sub-continent together comprise the NIO. The Indian sub-continent, as well as the NIO climate, is highly influenced and geared by the reversing Asian monsoon winds namely South–West and North–East monsoons (Schott and McCreary 2001; Anoop et al. 2015; Mahmood et al. 2018). In context to the South Indian Ocean (SIO, 70S: Equator, 20E:120E) the global wind belts govern the wind and wave climate knowingly trade winds and Southern Indian Ocean westerly (Young et al. 2011). The strong southwesterly winds in the NIO are caused by the East African highlands (Slingo et al. 2005) and it is the dominant mode of variability in the NIO (Anoop et al. 2015). Typically, the location in SIO bounded between the geographical coordinates 40° S–60° as well regions in the Southern Ocean (SO) south of 60° S is persistent with very strong westerlies, which are quite active in swell-generation and that propagates towards the NIO (Kurian et al. 2009; Nayak et al. 2013; Zheng et al. 2018). The AS was identified with the presence of 'Shamal' swells (Aboobacker et al. 2011; Aboobacker and Shanas 2018a) and Makran swells (Anoop et al. 2020), which attributes to the modification of the AS wave climate.

Based on the diversified wind characteristics in the entire IO domain, the regime is divided into six sub-domains, as shown in Fig. 1. Table 1 depicts the various sub-domain regions listed as follows: Region 1 (Arabian Sea), Region 2 (Bay of Bengal), Region 3 (South China Sea), Region 4 (Tropical South Indian Ocean), Region 5 (Western extra-tropical south Indian Ocean and Southern Ocean) and, Region 6 (Eastern extra-tropical south Indian Ocean and Southern Ocean). In a global study for swell waves by Alves (2006), the IO was sectored into three areas, such as the TNIO (Tropical North Indian Ocean), the TSIO (Tropical South Indian Ocean), and the ETSI (Extra-Tropical South Indian Ocean). This classification was based on the non-interrupted storm tracks, and the ETSI was zonally bounded between ~ 25° and 80° S. In the present study, sub-domains 5 and 6 together represent the zonal area between 35° and 63° S (collectively ETSI here onwards), in which the easterly winds over the TSIO and westerly winds in the extratropical region are mutually exclusive.

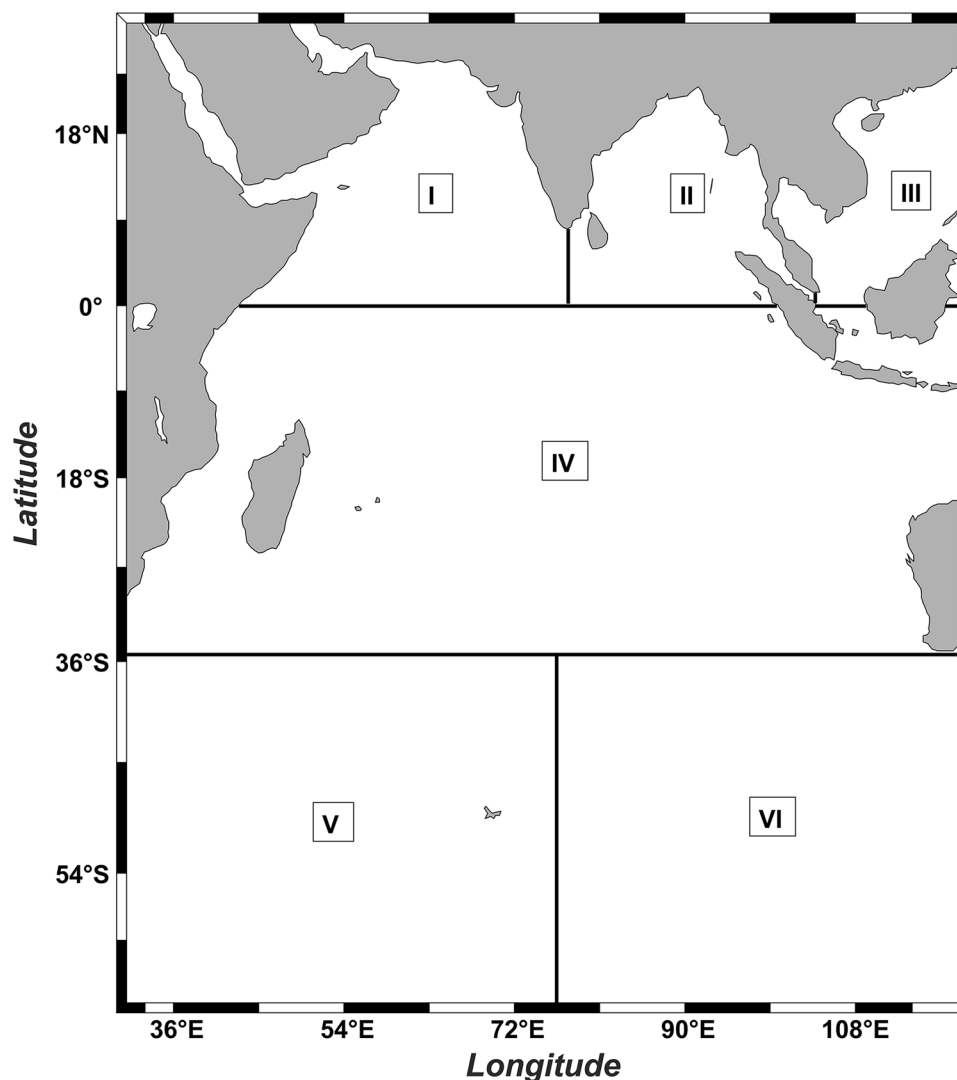**Fig. 1** Study area showing the Indian Ocean region divided into six sub-domains

Table 1 Description of the study area

Regions	Area description	Geographical coordinates (in deg)
Region 1	Arabian Sea	EQ: 30° N; 30° E:78° E
Region 2	Bay of Bengal	EQ: 30° N; 78° E: 105° E
Region 3	South China Sea	EQ: 30° N; 105° E: 120° E
Region 4	Tropical South Indian Ocean	35° S: EQ; 30° E: 120° E
Region 5	Western extra-tropical south Indian Ocean and Southern Ocean (south of 60° S)	63° S: 35° S; 30° E: 76° E
Region 6	Eastern extra-tropical south Indian Ocean and Southern Ocean (south of 60° S)	63° S: 35° S; 76° E: 120° E

3 Data and methodology

The IPCC Fifth Assessment Report has mentioned that no dataset is superior when all records have their benefits and limitations. Formulation of the current study was based on altimeter derived monthly averaged significant wave height observation, whereas ERA5 and WAVE WATCH III (WWIII) model data are used for a detailed comparison with the former one. Altimeter data covers 25 years (1992–2016) of continuous wave data whereas the WWIII and ERA 5 data provide 22 years (1997–2018) and 27 years (1992–2018) of wave records, respectively. The altimeter-derived significant wave height data is a calibrated and blended observation of nine multi-platform satellites. This composite and quality checked space-borne data of the nine altimeter missions (ERS-2, TOPEX/POSEIDON, GEOSAT Follow-ON (GFO), JASON-1/2, ENVISAT, CRYOSAT, and SARAL) is retrieved from the French Research Institute for Exploitation of the Sea (IFREMER/CERSAT). The BRAT (Basic

Radar Altimeter Toolbox) toolbox version 4.2 is employed to retrieve and post-process the raw swath data extracted from the satellites mentioned above into a gridded form and used for further analysis. It provides a better treatment of extrapolation with exception near the continental margins. The final processed monthly data obtained from BRAT comprises of H_S at a spatial homogeneity of $0.33° \times 0.33°$ horizontal grid resolution is used to investigate and establish the trends and wind-wave climate variability.

ERA5 is the fifth generation reanalysis data provided by ECMWF implementing substantial amendments to the existing assimilation system from the Integrated Forecasting System (IFS) Cycle 31r2–41r2. ERA5 dataset has advantages over ERA-interim for the modern parameterization techniques used, and the additional information on uncertainties in the reanalysis (Hoffmann et al. 2019). For ocean waves, ERA5 is available with spatial and temporal resolutions of 0.5° and 1 h, respectively and the present study utilizes 27 years of ERA5 reanalysis data from 1992 through 2018 retrieved from C3S. WWIII (Tolman 1991, 2009) is a third-generation phase-averaged wave model developed at NOAA/NCEP based on the action density balance equation. This study used the wave record from the NCEP global run of WWIII for a span of 22 years, which is provided by the Asia–Pacific Data Research Centre (http://apdrc.soest.hawaii.edu/datadoc/ww3.php) at a re-gridded spatial resolution of $1.25° \times 1°$. The wave prediction system of NCEP was developed using the analysis data from the global atmospheric forecasting system (GFS) at NCEP/NOAA (Moorthi et al. 2001). The spatially down-sampled records of significant wave heights from ERA5, WWIII, and satellite altimetry sources are compared using the following statistical analyses for the whole IO regime.

To compare the performance of reanalysis and model products with the space borne data, the following the quantitate assessments have been carried such as the correlation coefficient (r), the average absolute error (AE) (Stow et al. 2009).

$$r = \frac{\sum_{i=1}^{n} \left(Oi - \bar{O}\right)\left(Pi - \bar{P}\right)}{\sqrt{\sum_{i=1}^{n} \left(Oi - \bar{O}\right)^2 \sum_{i=1}^{n} \left(Pi - \bar{P}\right)^2}}$$

$$AE = \frac{\sum_{i=1}^{n} Pi - Oi}{n}$$

where n = the number of observations, Oi = the ith of n observations, Pi = the ith of n predictions, and $\bar{O}$ and $\bar{P}$ are the observation and prediction averages, respectively.

The correlation coefficient (r) pertains to the relationship of the relative movements of two variables and, the value ranges between − 1 and 1. The zero value infers no correlation and the positive sign indicates that the variables vary linearly. AE is the average magnitude of the residuals

(distance from the reference) regardless their direction of change in which individual elements is provided with equal weightage. It is worthwhile to perform a detailed investigation of the variability of waves in the identified sub-domains. In this study, the wind-wave characteristics over each sub-domain (Fig. 1) are examined in detail, seeking a better representation on the regional based wind-wave characteristics and their temporal variability. The annual variations in the average and maximum significant wave heights are estimated for the study regions. The regional monthly maximum (H_{SMAX}) wave heights for each sub-domain were derived from the monthly averaged data sets. H_{SMAX} is examined in two aspects, such as the annual averaged H_{SMAX} and annual maximum H_{SMAX} (annual maximum of monthly maximum). The investigation on the variability and characteristics of wind-waves includes monthly and seasonal climatological analysis, characteristics of seasonal cycle, segmented wave analysis ranging from 99th to 10th percentile H_S for each pentad time segments. 99th percentile is a statistical measure corresponding to a value below which 1% of the observations fall, and the percentile ranks are often recommended for extreme value analysis (Young et al. 2012). The pentad wave responses are described with the linear regression best-fitting trend lines, which attribute the change in wave height during the respective time window. Linear regression analysis is done using poly-fitting function and the slope of the linear fitting time series (y = mx + c; where m is the slope, c is the intercept, x is the time in years, and y the corresponding value of H_S), which provides the change per year.

4 Results and discussion

This section covers a comprehensive analysis on the wind-wave climate in the IO and provides a detailed description on the trends in a changing climate scenario. In a broader perspective, the discussions are made on aspects such as (1) the comparison study of synoptic annual trend analysis using different wind-wave datasets, (2) monthly and seasonal wave climatology for IO using 26 years of altimetry data, (3) characteristics of annual cycle in the regional basins, (4) monthly trends in wind-wave climate on a pentad scale.

4.1 Comparison study of synoptic annual trend analysis using different wind-wave datasets

The information on wind-waves has an immense application for wide range of offshore and ocean engineering related applications, and therefore datasets having substantial observation frequency and time domain will be an essential prerequisite to derive meaningful findings. The in situ buoy and ship observatory records are beneficial in location-specific investigations but unfit for regional studies. Spatially

homogenized data for a substantial period can be generated from satellite swath data and model-simulated data. In the past years, the developments in the earth observatory systems and model physics are remarkable. One can find more information from Bhaskaran (2019) concerned with the advancements and challenges in the wave modeling for IO.

This section compares the wave records of ERA 5, WWIII, and Altimeter derived H_S. Figure 2 demonstrates the annual variation of significant wave heights for every subsection that represents the overall trend of wind-waves based on the datasets mentioned above. Each subplot illustrates the annual response of synoptic mean, higher percentile waves (100th, 99th, 95th, and 90th), and annual maximum H_{SMAX}. The variable H_{SMAX} represents the monthly spatial maximum H_s for each sub-domain. Similarly, the higher percentile waves are the regional higher waves. On an annual scale, H_{SMAX} is analyzed in two aspects as annual averaged H_{SMAX} and annual maximum H_{SMAX}. Out of the three datasets, ERA5 and altimeter wave heights exhibit good correlation in regard of the mean H_S, 90th, 95th, and 99th percentile waves. The correlation coefficients of altimeter waves with ERA5 and WWIII are found to be 0.97 and 0.94, respectively. Figure 3 shows the scatterplots of ERA5 and WW3 with altimeter H_S. The agreement of ERA5 and altimeter annual average H_S is very good whereas, the correlation of WWIII with altimeter higher waves (99th, 95th, and 90th
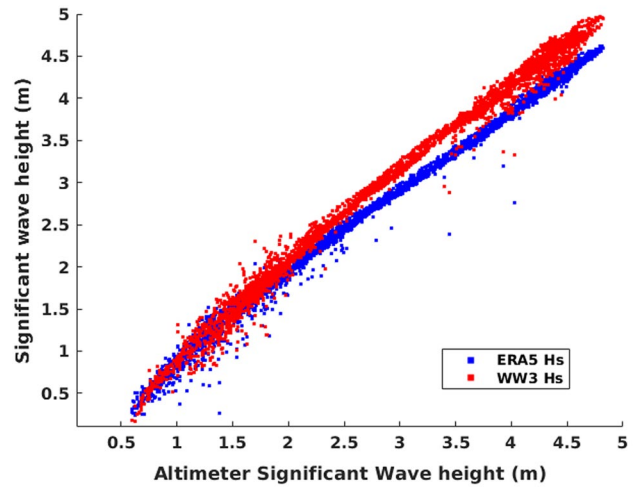

Fig. 3 Scatterplot between Altimeter HS and (blue dot) ERA5, and (red dot) WW3 HS

percentile waves) is moderately good in the Arabian Sea, BoB, and the TSIO during the years 1997 and 2007 (not shown in this paper). The time series of annual maximum H_S (100th, 99th, 95th, and 90th percentile waves) in all regions exhibits a high degree of variability as compared to the annual minima. Specifically, the higher wind-waves in IO regime are more prone to the impact from climate change.

Fig. 2 Trends in the annual maxima, 99th, 95th, 90th percentile and annual mean responses of altimeter, ERA5, and WWIII HS for Regions 1–6
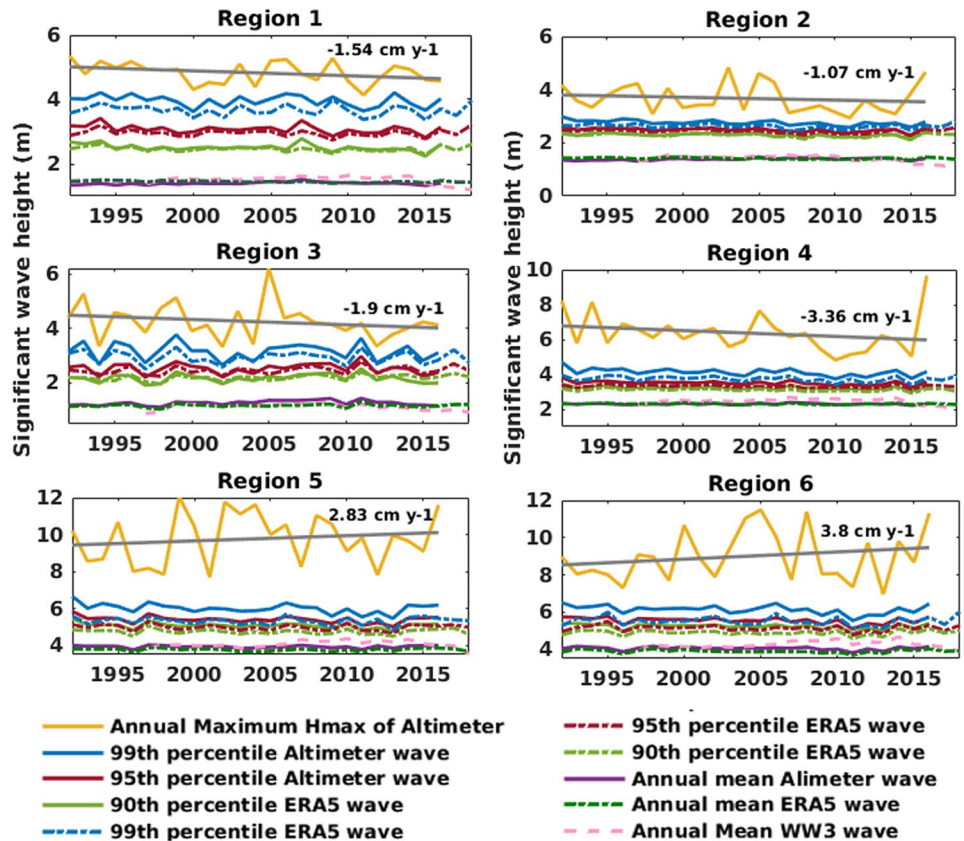
The annual trends are well captured by all three datasets but it is observed that the ERA5 underestimates the higher waves, particularly the 95th percentiles H_S (Fig. 2).

Figure 3 show the scatterplot of ERA5 and WWIII with altimeter HS. As seen there is under-estimation of ERA5 Hs for higher waves, whereas the Hs of WWIII is observed in the range of altimeter and consistent with other studies (Stopa and Cheung 2014a; Stopa et al. 2019). The quality of wave model forecasts depends on the quality of the input wind forcing data. The ECMWF wind product seems to underestimate extreme events (Stopa and Cheung 2014b) whereas, the WWIII utilizes Climate Forecast System Reanalysis (CFSR) surface winds in which the extreme events are generally well captured. In context to higher waves, for the NIO and TSIO, the 90th and 95th percentile waves are found to be synchronous and in-phase with the observed waves, whereas the 99th percentile waves are underestimated. The maximum underestimation of ERA5 is noticed for higher H_S in the ETSI (Fig. 2, regions 5, and 6). A global evaluation of ERA-5 wind and wave has demonstrated that the maximum errors in ERA5 are associated with the extreme sea-states of extra-tropical systems, and tropical cyclones (Parsons et al. 2018). In a similar context, the ERA5 H_S during the Phailin cyclone has underestimated the buoy data located at Gopalpur (Muhammed Naseef and Sanil Kumar 2019).

In the NIO, the AE for ERA5 H_{SMAX} was found 0.65 m, whereas it is more than 1 m in the TSIO (1.27 m), the western ETSI (1.9 m), and the eastern ETSI (1.65 m). Similarly, the AE for ERA5 H_{SMAX} are: the BoB (0.9 m), the TSIO (1.92 m), the western ETSI (4.09 m), and the eastern ETSI (3.09 m). The ERA5 H_S showed an excellent correlation with altimeter H_S, however, the waves higher than 95th percentiles are under-estimated in all sub-domains of the IO. The lower resolution of ERA5 ($0.5° \times 0.5°$) compared to the altimeter data ($0.33° \times 0.33°$) exhibits lower maximum values. Nevertheless, the ERA5 data is highly beneficial for long-term trend analysis attributed due to good correlation with the observations. In the NIO, the errors are found minimal, and for fair-weather conditions the ERA5 is highly recommended.

Table 3 describes the regional differences of the synoptic annual wave trends of altimeter H_S and H_{SMAX}. Interestingly, the altimeter annual averaged H_{SMAX} and annual maximum higher waves (99th and 95th) exhibit a decreasing trend in all the six domains from 1992 to 2016 (Table 3). The decreasing trend is consistent with the findings of Muhammed Naseef and Sanil Kumar (2019), in which the annual mean and annual maximum H_S for IO was observed to be decreased during 1991–2016. The declining rate of annual averaged H_{SMAX} is worth noticing in the TSIO, the western ETSI and AS such as 2.3 cm/year, 2.2 cm/year, and 1.9 cm/year, respectively. At the same time, the annual maximum H_{SMAX}

showed an increasing wave trend measured as 2.8 cm/year and 3.8 cm/year respectively in the western and eastern parts of the ETSI.

4.2 Monthly and seasonal wind-wave climate

Figures 4 and 5 illustrate the long-term monthly and seasonal wave climate for the IO using 25 years of satellite altimetry data. When the ETSI sector experienced an average H_S of 4.0–5.0 m during January and February, the mean H_S in the AS and BoB varied between 0.8–1.5 and 1–1.5 m, respectively. In March and April, the SO storm belt has a mean H_S of about 5.0 m, and the maximum wave height is seen in the eastern ETSI. In April, a substantial wave interference with local wind-seas is visible in the Bay of Bengal, off Somalia coast, south–west, and southeast coasts of the Indian subcontinent with a mean Hs range of 2.5–3.5 m. The Bay of Bengal experiences a seasonal higher wave field in the order of about 3 m during the peak SW monsoon, and that recedes during the post-monsoon phase. The SW monsoon steers high wave field in the Head Bay region. It is worth noticing that most of the time (September–April), the central and south BoB experienced relatively higher mean H_S compared to the Head Bay of Bengal even during the onset and the withdrawal phase of SW monsoon. The wave activity in the central and southern BoB is identified to be high, particularly when the mean H_S in the ETSI are higher than 5.5 m. However, during the peak SW monsoon, the mean H_S in the head Bay, the central, and south BoB is within the range of 3 m. Earlier studies have established the fact that storm outbreaks in the ETSI generate swell wave field that eventually propagates crossing the hemisphere. The swell wave field that propagates from this region modulates and modifies the local wind-wave conditions in the NIO regime (Nayak et al. 2013; Remya et al. 2016). Remya et al. (2016) also reported that high swell activity in the Andaman Nicobar coast, east and northeast coasts of the IO (2–3 m), and the swell wave fields at Oman coasts are associated with the ETSI extreme wave activity. Moreover, the wave activity in April over the AS and BoB matches with the operational wave forecast provided by INCOIS, Hyderabad, for the east coast of India (https://incois.gov.in/portal/ osf/hwa.jsp; https://www.thehindu.com/news/national/swell-waves-forecast-along-indias-coasts/article23620-767.ece, published on April 20, 2018).

The reversing monsoon wind system characterizes the local wind-wave climate for the NIO. During northern winter, dry surface air blows from land to sea in the northeast direction, resulting in the northeast monsoon season, and in summer there is a complete reversal of the wind system with moist winds blowing from sea to land along the south-west direction, resulting in the south-west monsoon season. Further, a significant wave activity is observed in the north AS during April, and its propagation towards
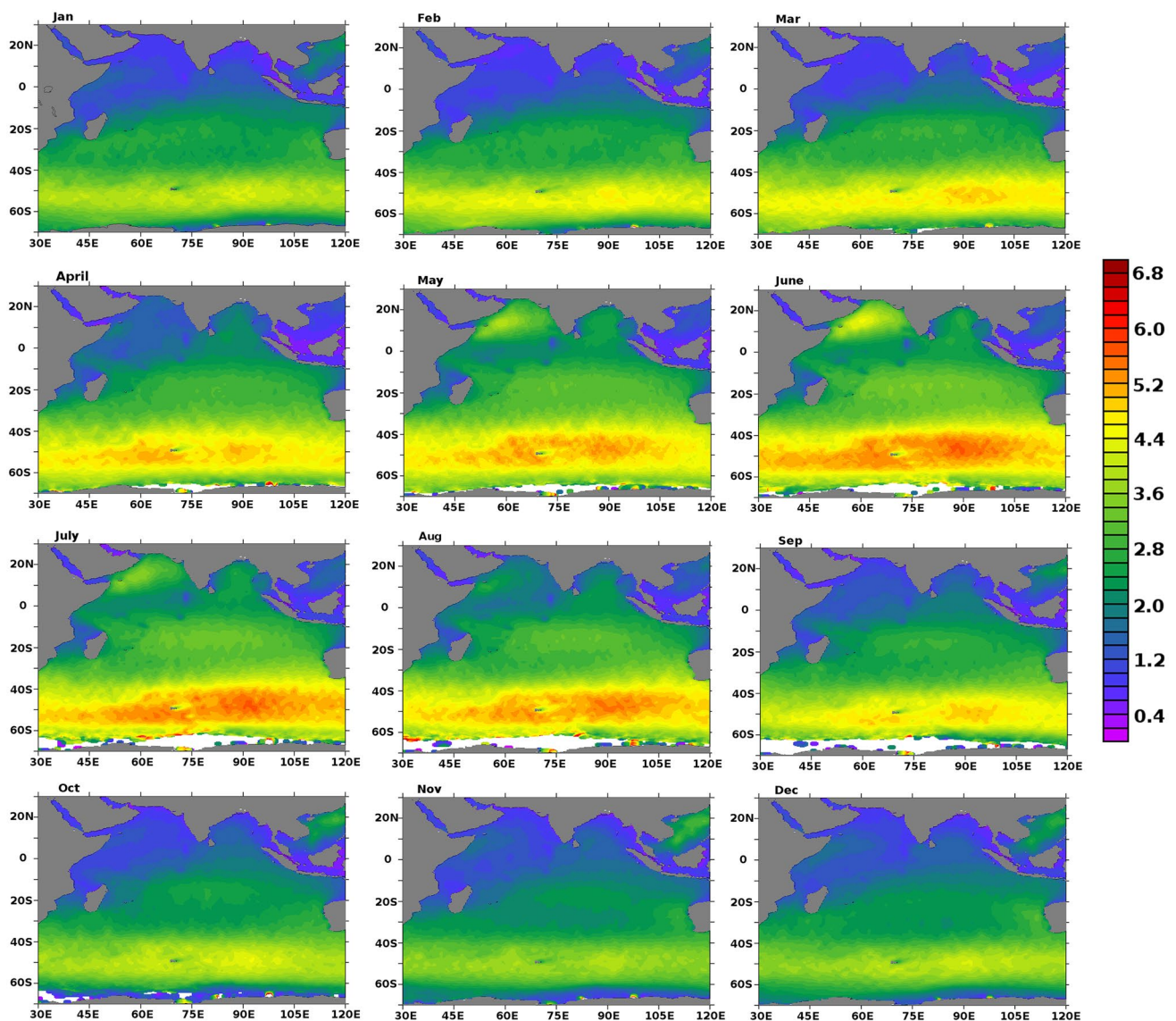
Fig. 4 Climatology of monthly mean significant wave height for the Indian Ocean region

the west coast of India. The wave activity in the north AS was reported to be associated with the *Shamal* waves and *Makran* waves (Aboobacker and Shanas 2018b). The significant wave height (~ 3.5 m) also agrees with the findings, as reported by Aboobacker and Shanas (2018b). The months of November, December, and January exhibit relatively calm wave activity in the NIO, the TSIO, and the ETSI experiences a maximum H_S of 4.0 m. The South China Sea experiences higher wave activity from September to February ranging between 3 and 4 m. The ETSI has the strongest wave field over the entire IO, and the location corresponding to 90° E and 50° S recorded the highest mean about 6 m during the austral winter (April–October).

4.3 Characteristic of seasonal cycles

The regional variations in the wind patterns along with the active global wind belts directly influence the wind-wave climate in basin-scale and that for the NIO; the former plays an inevitable role, though the participation of distant winds is significantly concerned with swell waves. Analysis of the annual cycle considering datasets spanning a considerable length of time can provide vital information on the regional wind-wave climate and the most frequent wave heights existent in that region. In the same context, Zheng et al. (2016b) studied the wave energy distribution on a global scale by running the WWIII model
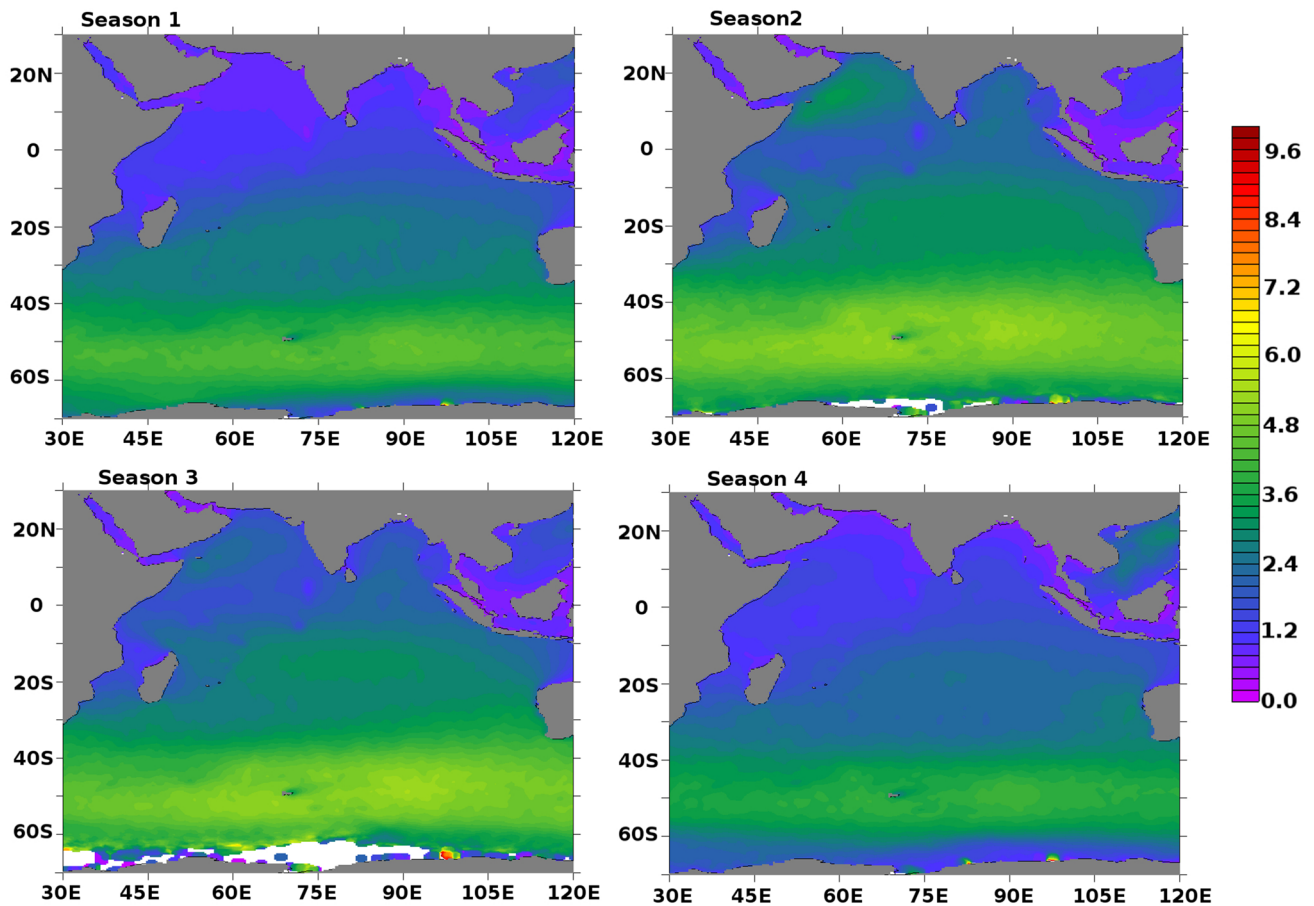
Fig. 5 Seasonal distribution of significant wave height (in m) for the Indian Ocean region

for 1 year. It was found that JJA (June, July, and August) is recorded with the highest seasonal wave mean in the southern hemisphere, and the wave energy is perpetually distributed along with the south-westerlies. Whereas in the northern hemisphere, wave energy was found concentrated in the northern Atlantic and Pacific oceans, and the values were observed highest in DJF (December January, February). This section emphasizes the existing knowledge in the monthly wind-wave activity in the IO and, the study conducted at regional scale using altimeter wave heights. Figure 6 shows the long-term seasonal cycle of 99th, 95th, 90th, 75th, 50th, 25th, and 10th percentiles of H_S and each subplot representing the identified sub-domains of IO. Table 2 provides information on the various confidence limits of H_S in the six sub-domains based on the analysis of 25 years of satellite data, which are used to establish the seasonal cycles of the respective domains. Indeed the seasonal dependence and the percentage occurrence of H_S from January to December delineate their contribution to the annual wave statistics. For all regions except the South China Sea (R5), the seasonal activity begins in May–June,

continuing up to the months of September–October, where the maxima occur during July. The higher waves (greater than 90 percentiles H_S) are recorded active during October to February in the SCS, and the maximum H_S are much frequent in December. Remarkably, for the Arabian Sea, the 99th percentile waves are concentrated during July with an occurrence frequency of about 80%. For Western and Eastern Extra-tropical South Indian Ocean, the seasonal activity lasts for about 6–7 months (April–October). High percentile waves are less evenly distributed over the months, and lower percentile waves (≥ 25th percentile H_S) exhibit a constant distribution along all months, particularly in the regions of the NIO and the TSIO. From the wind-wave climate study, it can be inferred that all regions except the BoB account for H_S excess of 5.0 m during the period 1992–2016. In particular, the SO storm belt imparts a higher risk of swell generation, and propagation towards the NIO as the higher confidence limit distributions lies in the range of 10–30% for 5–6 months, wherein the wave heights are remarkably higher (4.0–6.0 m) (Table 3).
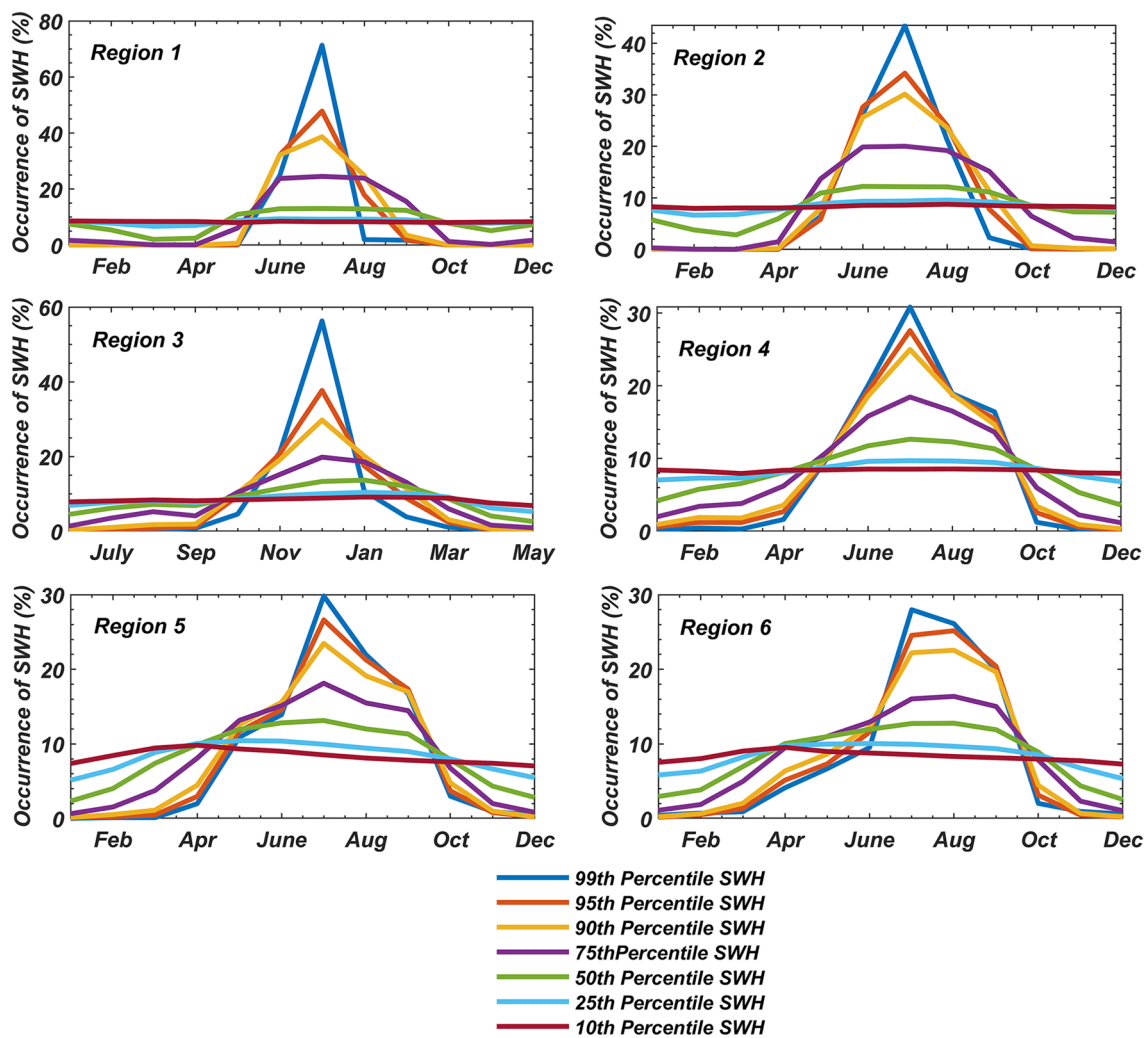
Fig. 6 Seasonal cycles of the 99th, 95th, 90th, 75th, 50th, 25th, and 10th percentile SWH for Regions 1–6

Table 2 Distribution of various confidence limits of SWH for different sub-domains of Indian Ocean

Confidence limits of SWH	Region 1	Region 2	Region 3	Region 4	Region 5	Region 6
99th	3.955033	2.770986	3.210855	4.139047	6.050194	6.172355
95th	3.069461	2.489617	2.536957	3.499182	5.400422	5.557634
90th	2.497742	2.299484	2.178066	3.234107	5.065907	5.230472
75th	1.700689	1.825177	1.615122	2.815611	4.504258	4.670168
50th	1.152074	1.321865	1.126638	2.347538	3.878087	4.02856
25th	0.867783	0.863192	0.916323	2.257399	3.284272	3.397189
10th	0.665232	0.62148	0.58616	1.202222	2.805733	2.843675

4.4 Pentad scale wave analysis

4.4.1 Arabian Sea (Region 1)

The AS is a part of the semi-marginal seas in the NIO, and three major weather systems control the dynamics,

knowingly pre-monsoon, monsoon, and post-monsoon seasons. For the Arabian Sea, the trend in monthly maxima H_S was reported increasing during the period from 1992 to 2012 in a comprehensive study conducted for fair weather conditions (Gupta et al. 2015). This section demonstrates the temporal variability of segregated monthly mean H_S

Table 3 Wind-wave trends in different regions of Indian Ocean during 1992–2016

	Region1 (cm/year)	Region2 (cm/year)	Region3 (cm/year)	Region4 (cm/year)	Region5 (cm/year)	Region6 (cm/year)
Annual maximum H_{max}	− 1.54	− 1.07	− 1.9	− 3.36	+2.83	+3.8
Annual averaged H_{max}	− 1.96	− 1.05	− 1.15	− 2.4	− 2.21	− 1.48
99th percentile H_S	− 0.72252	− 0.82401	− 0.49871	− 1.57461	− 1.40003	− 1.31487
95th percentile H_S	− 0.67638	− 0.54486	− 0.06587	− 0.89492	− 0.90726	− 0.94589
90th percentile H_S	− 0.61107	− 0.43201	0.0671	− 0.6181	− 0.69197	− 0.6579
Annual mean H_S	0.180502	0.273554	0.371431	− 0.07785	− 0.06475	− 0.27517

for every 5 years in the AS. Therefore, this study will be beneficial to understand the short-term changes that occurred in the climatological scale. The sub-plots shown in Fig. 7 portrays the pentadal variations of 99th, 90th, 75th, 50th, 25th, and 10th percentile H_S together with linear regression fit representing the rate of annual change. The study finds the variation to be significant for different wave range bins from the 99th to 10th percentile H_S levels. The pentad plots corresponding to the period from 2007 to

2016 exhibit a stabilized wave trend in the range between 0.8 and 4.5 m.

Interestingly, from Figs. 6a and 7a–f, the higher threshold waves, within the limits of 99th to 50th percentile H_S (1.7–5.0 m), are primarily influenced by the seasonal winds whereas the 10th and 25th percentile H_S (0.5–1.0 m) manifest small or no dependency. Even though the monsoonal winds are the dominant mode of wind-wave variability, local winds are found to steer the lower percentile waves. The AS
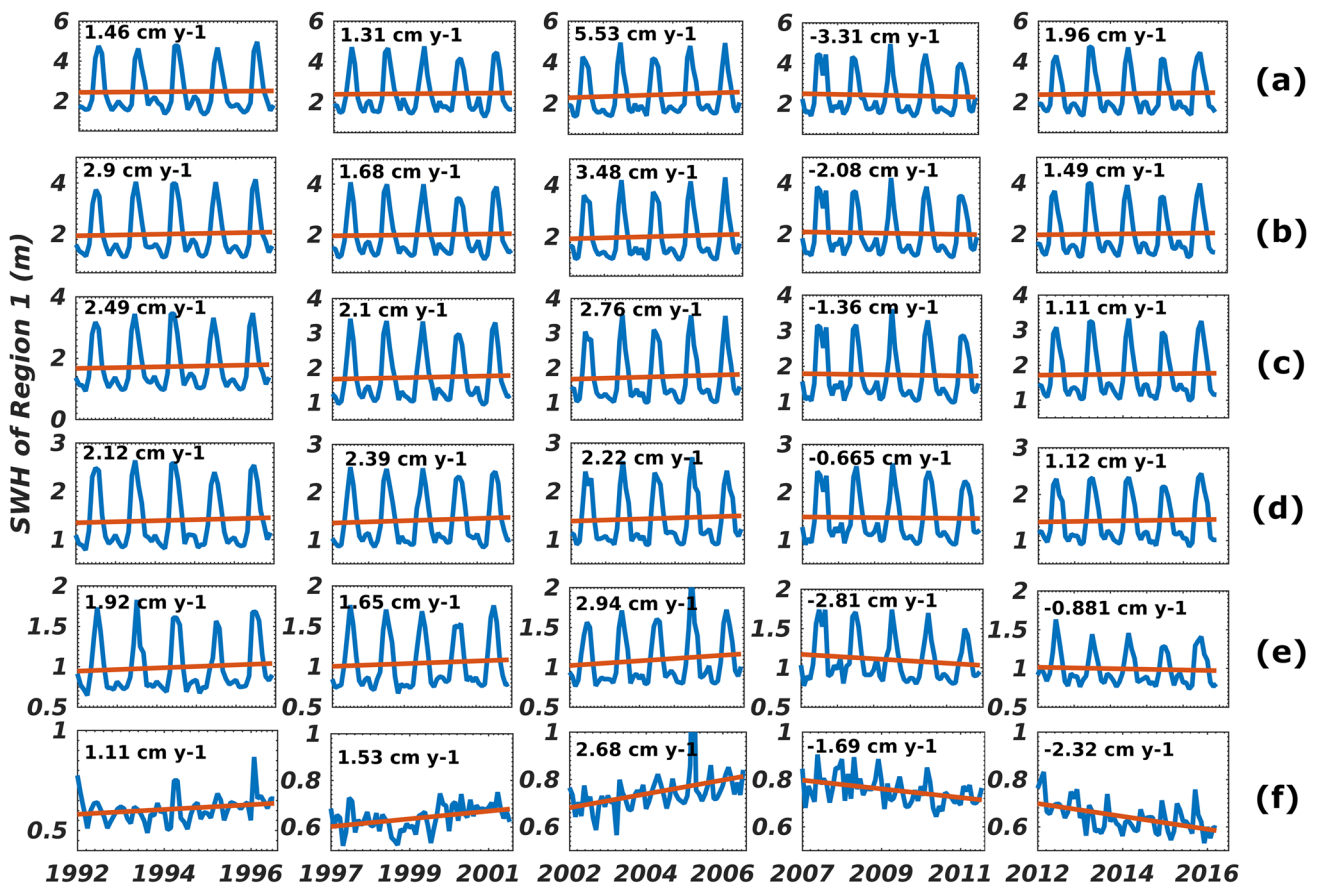

Fig. 7 Pentad variation plots of **a** 99th percentile, **b** 90th percentile, **c** 75th percentile, **d** 50th percentile, **e** 25th percentile, **f** 10th percentile SWH values for Region 1 during 1992–2016

exhibited a decadal cycle during 1997–2016, and the same trend is noticed for the BoB and SCS. From the five consequent pentad analyses from 1992 to 2016, the AS showed a maximum positive trend (5.53 cm/year) during 2002–2007 and decreased during the period 2007–2011 (− 3.31 cm/year).

4.4.2 Bay of Bengal (Region 2)

In the context of global warming and its repercussions on increased SST (Sea Surface Temperature), the Bay of Bengal is more prone to tropical cyclogenesis, and in the recent climate change scenario, the intensity of tropical cyclones is also found to increase. Nevertheless, the amplitude of predominant waves was reported being lower in the Bay of Bengal sector (Chandramohan et al. 1990; Vethamony et al. 2000) wherein above one-third waves occur in the range between 1.0 and 1.5 m in a year. Figure 8 pertains to the temporal variability of segmented H_S in the pentad scale from 1992 to 2016 in the BoB. The 90th and 99th H_S ranges

between 1.0–3.0 and 1.0–3.5 m, respectively. The variability is independent of seasonal variation for lower confidence limits (10th, 25th percentile H_S) and thus do not follow the same trend as of higher percentile values (99th, 90th, 75th, 50th) in which the changes during the monsoon and post-monsoon seasons are positive and high. Interestingly, all the pentad trends have shown a positive rise for the 99th–50th percentile H_S, whereas a slight negative trend is observed for 25th–10th percentile values (Fig. 8e, f). It is essential to consider the patterns of extreme waves in the Bay of Bengal, as well as the frequency of occurrence of different wave regimes for practical use.

4.4.3 The South China Sea

The SCS is a semi-enclosed basin that forms a part of both the Pacific and the IO. Amongst the four seasons (spring, summer, autumn, winter) observed over this region, the H_S variability is more significant during winter as compared to summer. It was reported that winter (DJF) possess
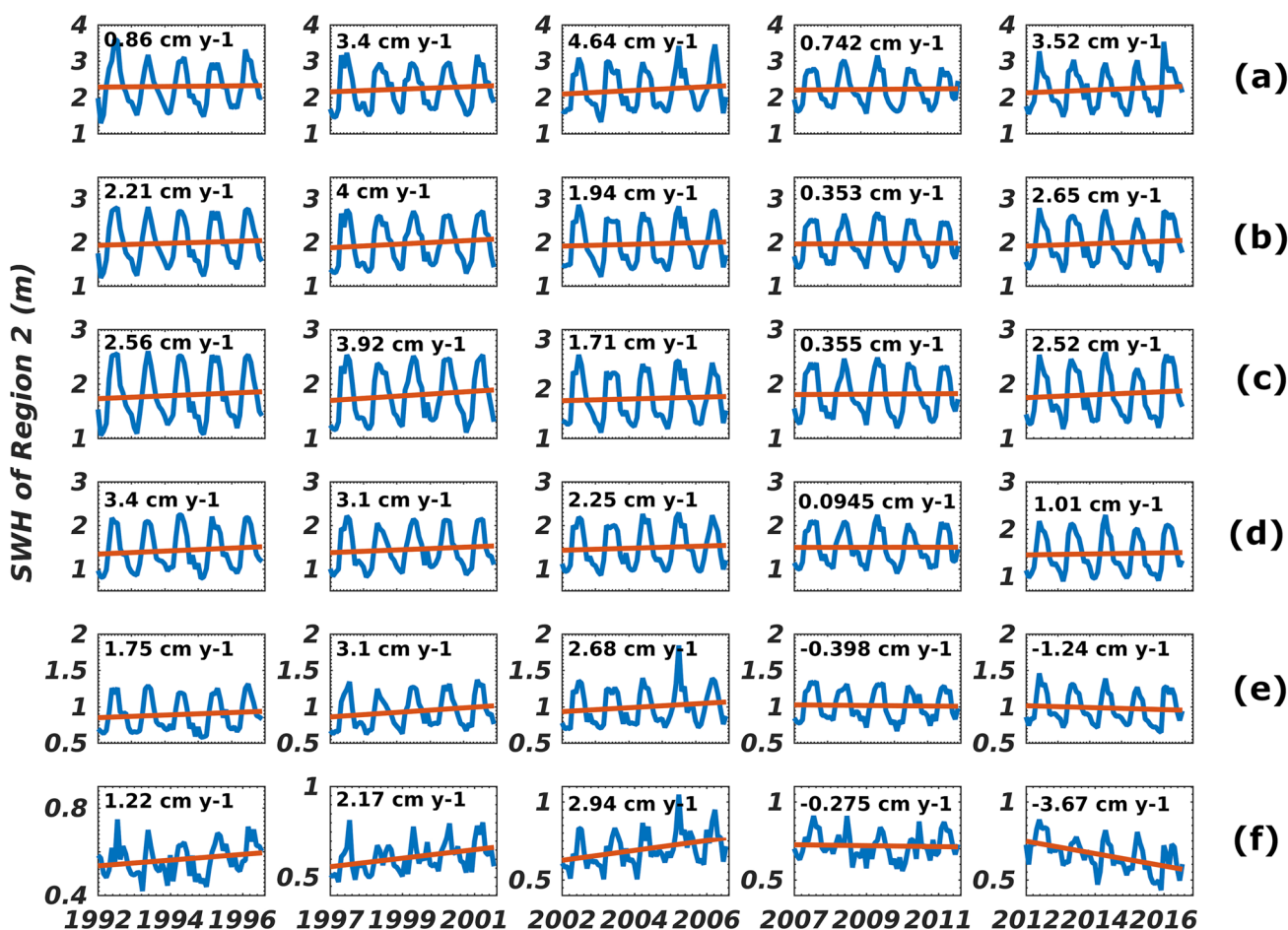

Fig. 8 Pentad variation plots of **a** 99th percentile, **b** 90th percentile, **c** 75th percentile, **d** 50th percentile, **e** 25th percentile, **f** 10th percentile SWH values for Region 2 during 1992–2016

higher wave power density with 15–27 KW/m, whereas for the autumn (SON) it is about 9–27 KW/m (Galanis et al. 2012; Lin et al. 2017). The inter-annual seasonal cycles exhibit a wide variability for higher waves that is evident in Fig. 9a–f. The range of 99th percentile values during the pentad 2012–2016 was observed to decrease for the range of 1.0–4.0 m, whereas it ranges between 1.0 and 5.0 m in the pentad period 1992–1996. Even though the observed variability is stabilized for the last two pentads (2007–2016), compared to the Arabian Sea and Bay of Bengal, the rate of increment per year was significant, ranging between 3 and 12 cm/year for the 99th to 50th percentile wave heights. A closer observation with the pentad time-series revealed a reversing trend in the later decadal time window, which was found to be more or less stabilized. The lower confidence limits (Fig. 9e, f) exhibit further decrement irrespective of relative higher variations. It implies that when the overall trend of wind climate decreased and shifted its range to lower limits, the variability of wave climate was observed to shift towards the lower percentile wave heights significantly.

4.4.4 Tropical South Indian Ocean

The sub-plots shown in Fig. 10 represent the variability corresponding to the range from 99th percentile to 10th percentile H_S analyzed for 25 years measured data in the TSIO. It is evident from the figure that the range of H_S has decreased during 2012–2016 at all levels of H_S (99th to 10th percentile H_S) as compared to the period 1992–1996. However, there is an increasing trend noticed in the last pentad (2012–2016), and the highest monthly mean H_S coincides with the strong El Niño years (2015–2016) (https://origin.cpc.ncep.noaa.gov/) and negative IOD event (2016) (http://www.bom.gov.au/climate/iod/). During 2007 and 2011, the TSIO experienced the highest decreasing wave trend measured around 9 cm/year, and the same is noticed in the ETSI, and AS. It is worth noticing that declining wave activity occurred during the strong La Niña periods (2007–2012) (https://origin.cpc.ncep.noaa.gov/). However, the increasing/decreasing trend in the Indian Ocean (especially the NIO) is not necessarily linked to El Niño/La Niña because the IOD also plays a
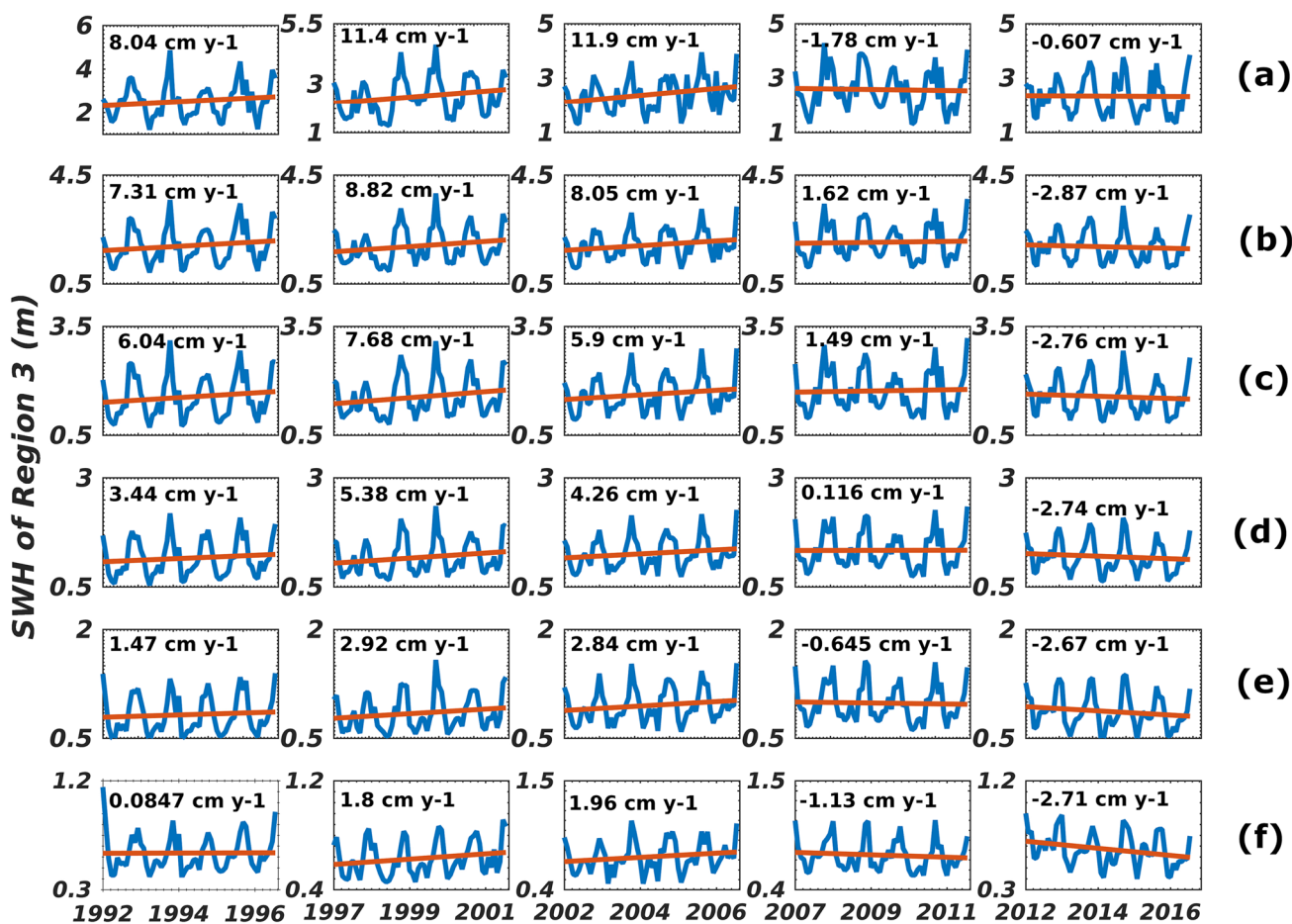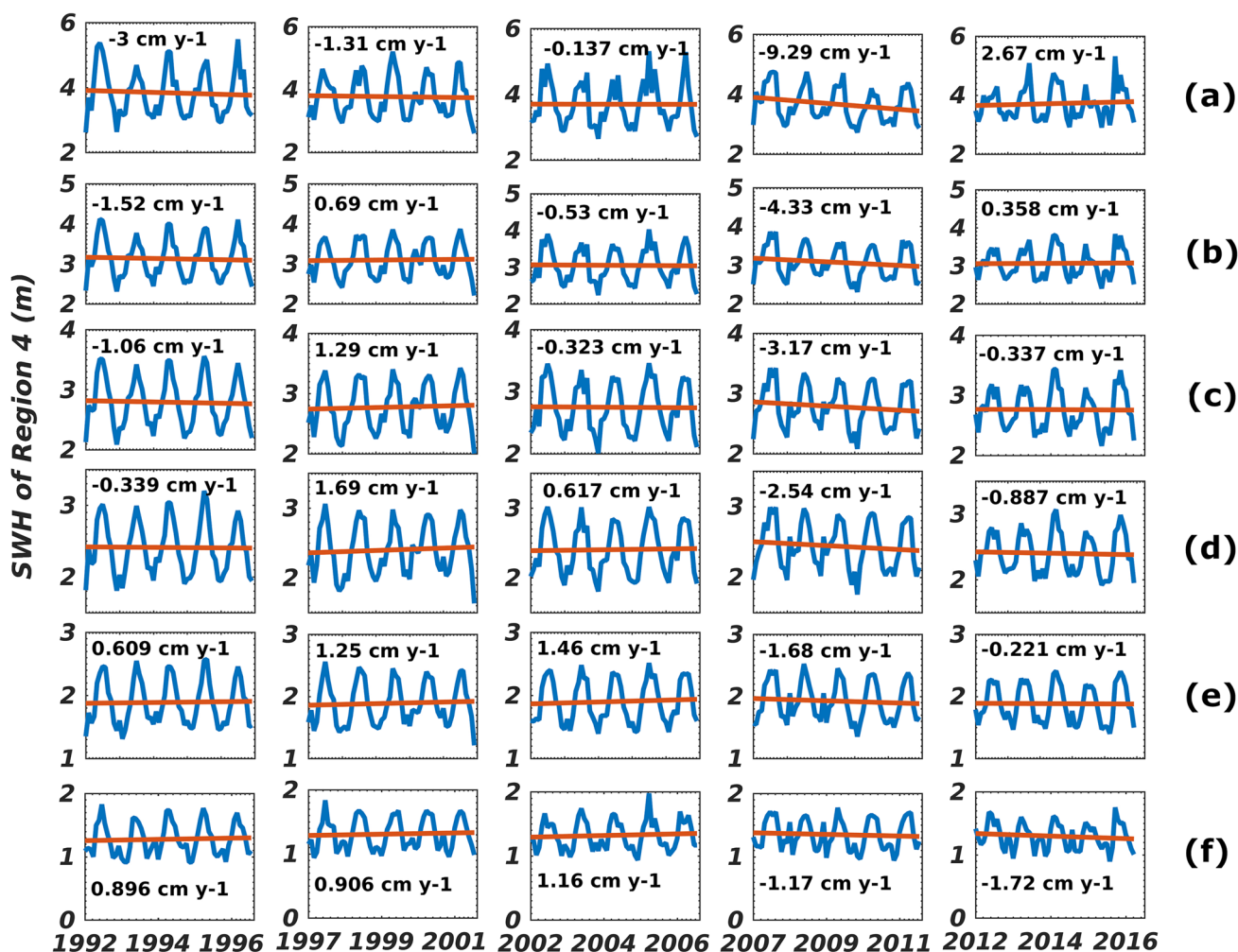

Fig. 9 Pentad variation plots of **a** 99th percentile, **b** 90th percentile, **c** 75th percentile, **d** 50th percentile, **e** 25th percentile, **f** 10th percentile SWH values for Region 3 during 1992–2016

Fig. 10 Pentad variation plots of **a** 99th percentile, **b** 90th percentile, **c** 75th percentile, **d** 50th percentile, **e** 25th percentile, **f** 10th percentile SWH values for Region 4 during 1992–2016

significant role in modifying the wind-patterns. The Indian Ocean Dipole (IOD) can also play a significant role in influencing the wave climate of the north Indian Ocean region. The study by Anoop et al. (2016) using measured, modeled and reanalysis wind and wave data examined the inter-annual mode of IOD variability on the wave climate of eastern Arabian Sea. Significant findings from their study indicates that the IOD induced changes in the equatorial sea surface temperature and sea level pressure leads to modification of the wind field in the northern Arabian Sea thereby causing inter-annual variability in the wave climate over the eastern Arabian Sea. The study indicates that IOD has a significant influence on the wave climate off the central west coast of India as compared to the northern and southern regions. These changes in the wind field due to IOD in turn influences the generation and dissipation characteristics of the wave field thereby causing a decrease in the northwest short period waves during positive IOD and an increase during the

negative IOD period (Anoop et al. 2016). Another study by Shanas et al. (2017) showed that climate indices such as the North Atlantic Oscillation (NAO) and the El-Nino–Southern Oscillation (ENSO) have a significant positive and negative correlation with the wave height characteristics in the northern and southern regions of the Red Sea. Notable features in their study show significant negative trends of Hs (99th percentile, 90th percentile, and mean) in the northern Red Sea during summer season, whereas significant positive trends are seen in the southern Red Sea during winter and the presummer season. Also their study establishes the fact that southern regions of the Red Sea have a strong linkage with IOD and that is consistent with the observed correlations in the Arabian Sea (Shanas et al. 2017).

Nevertheless, the observed changes in the TSIO very much synchronized with that of the ETSI and explained in the following section. Similar to the regions 1 and 2, the variability found marginal in all pentads except 2007–2011.

There is a decadal variability noticed at the lower percentile waves (10th, 25th, and 50th) during 1997–2016, irrespective of discrepancies at the higher levels. On average, the 99th percentile waves of the TSIO exhibits a decreasing trend in almost all pentads (Fig. 10), which is furthermore consistent with the negative annual maximum H_{SMAX} trend (3.36 cm/year).

4.4.5 Western and eastern extra-tropical South Indian Ocean

It is evident from Figs. 11 and 12 (Regions 5 and 6) that the Antarctica continent experience strong austral winter (June–September) and austral summer (November–February) seasons. In the IO basin, the ETSI sector has the strongest wind system (SO storm belt). Figures 10 and 11 are the pentad variations noticed for the period from 1992 to 2016, and each panel represents the variability at different confidence levels starting from 99th to 10th percentile values of H_S. It has been observed from the recorded data that wave amplitudes are slightly higher in the Region 6 as compared to Region 5. However, the rate of variability is higher (Figs. 11, 12) in the Region 5 as compared to Region 6. Variability in terms of rate of change of wave height per year is also significantly higher (4–13 cm/year) for the 99th to 75th percentile values, and that for the 10th–25th percentile waves are found to be less than 2 cm/year. For the two sectors of ETSI, there is a noticeable pentad cycle in the H_S from 1997 to 2016 with significant rates, and the cycle is valid through maximum to minimum H_S, especially in the western sector. In the SIO, a depression in the wave activity was found during 2007 and 2011, where the value is prominent in Region 5 (11.8 cm/year), and 6 (7.6 cm/year), and the decreasing
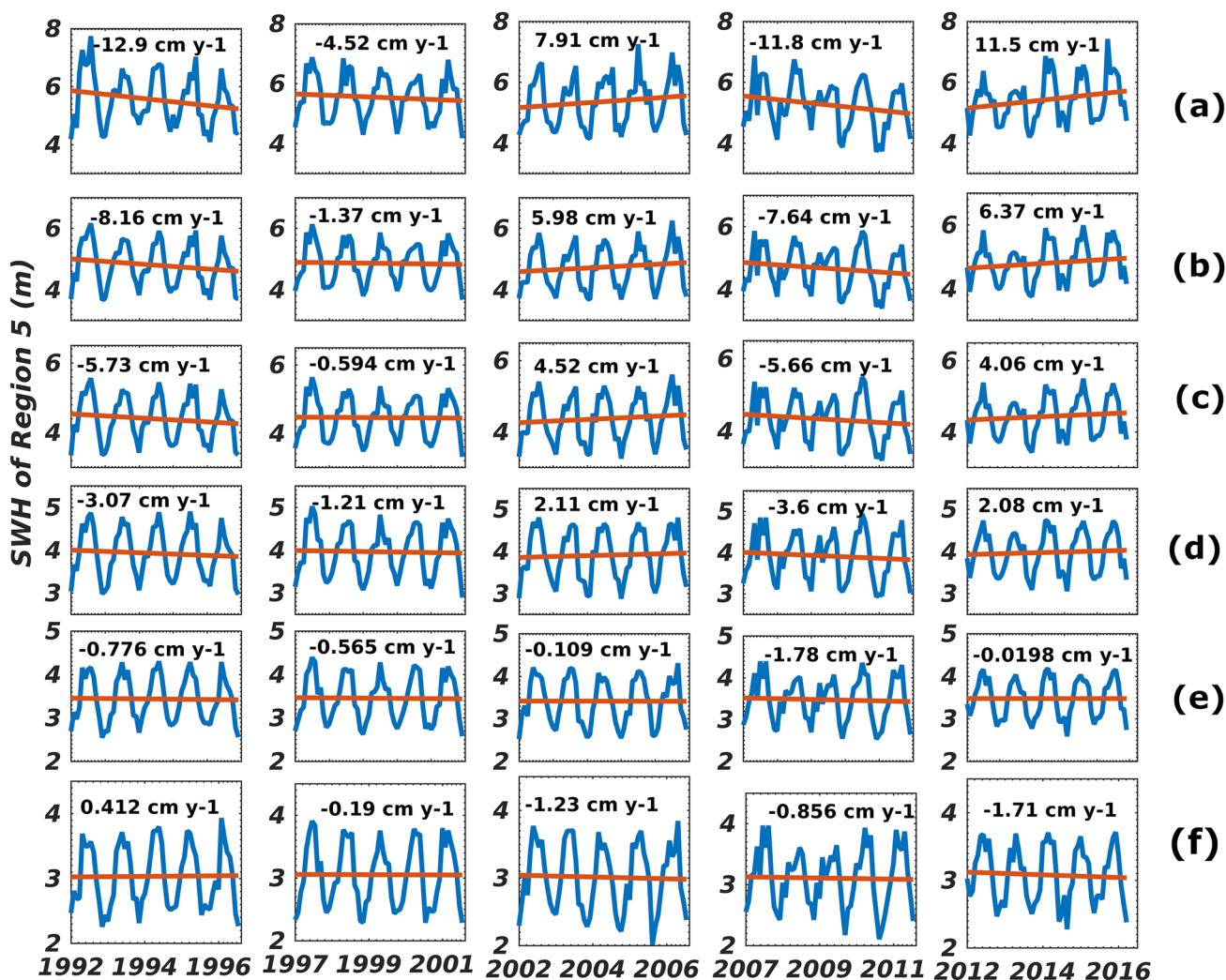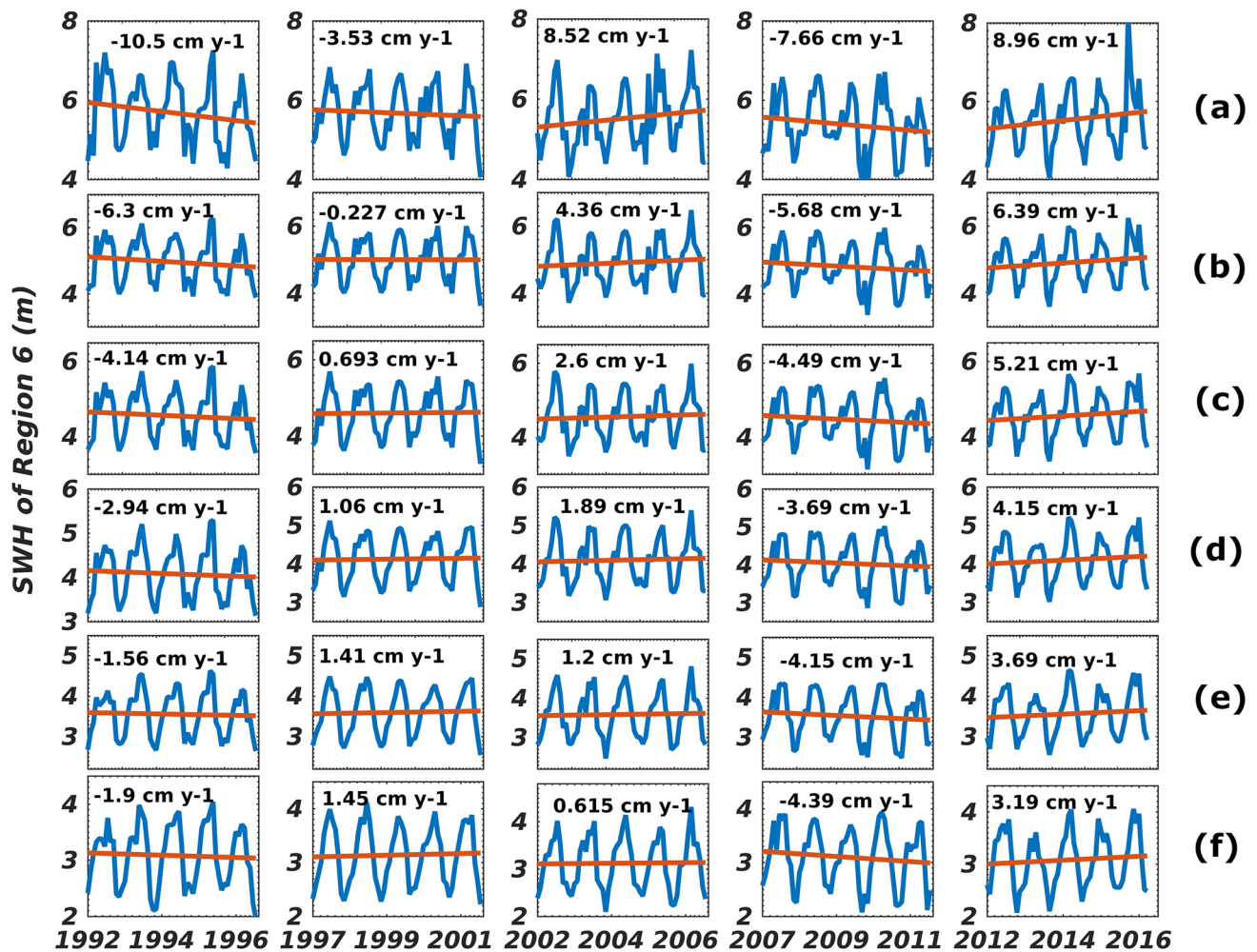

Fig. 11 Pentad variation plots of **a** 99th percentile, **b** 90th percentile, **c** 75th percentile, **d** 50th percentile, **e** 25th percentile, **f** 10th percentile SWH values for Region 5 during 1992–2016

Fig. 12 Pentad variation plots of **a** 99th percentile, **b** 90th percentile, **c** 75th percentile, **d** 50th percentile, **e** 25th percentile, **f** 10th percentile SWH values for Region 6 during 1992–2016

trend was also reflected in the AS during the same period. Based on Oceanic Niño Index (ONI) (https://origin.cpc.ncep.noaa.gov/), 2007–2011 years are observed as the dominant La Nina period, during which 2007–2008 and 2010–2011 are recorded as the strong La Niña events (https://ggweather.com/enso/oni.htm), whereas 2008–2009 is weak. During 1992–2016, there are two major El Niño events recorded of which 1997–1998 and 2015–2016 and categorized as very strong. In the ETSI, TSIO, AS, and BoB (Figs. 7, 8, 10, 11, 12), during 2012–2016, the variation in H_S increased during the period of strong El Niño cycle. During the same period in the TSIO and ETSI, the maximum mean H_S is recorded in the year 2016. According to a recent study on the influence of climate indices in the IO, during June–August, the ENSO influence on mean H_S is reported significant in the NIO and partially in the ETSI and TSIO (Kumar et al. 2019). Also, the Southern Annular Mode (SAM) influence on the mean H_S during

September–November is demonstrated to be significant in the ETSI, TSIO, and AS.

5 Conclusions

This study investigated the wind-wave characteristics of the Indian Ocean (IO) domain grouped into six sub-domains using the historical satellite altimeter records from 1992 to 2016. In the IO, the altimeter derived significant wave height (H_S) exhibited a good correlation with ERA5 (0.97) and WWIII (0.94) datasets. However, the later both datasets underestimate the annual maximum and annual average H_{SMAX} as compared to altimeter. The absolute average error (AE) for ERA5 was more than 1 m in the TSIO (1.27 m, 1.92 m), the western ETSI (1.9 m, 4.09 m), and the eastern ETSI (1.65 m, 3.09 m) when the annual averaged and annual maximum H_{SMAX} were consecutively considered. Therefore,

the study used altimeter wave data for further analyses of wind-waves. The wave heights were segregated into percentile ranks (99th–10th) for each identified region. The annual maximum H_{SMAX} in the western and eastern sectors of the ETSI show an increase of 2.83 cm/year and 3.8 cm/year, respectively. At the same time, the annual averaged H_{SMAX} was seen to decrease in all sectors of IO such as the TSIO (2.3 cm/year), the AS (1.96 cm/year), and the western ETSI (2.16 cm/year). Using the 25 years of monthly mean H_S record, the characteristic seasonal cycle of each segregated wave heights are studied for the sub-domains. The seasonal cycles of H_S indicates that the frequency of percentage occurrence of 99th HS is broadly distributed for the ETSI (from April to October) whereas, it is steep and narrow in the AS, designating the strong influence of Southwest monsoon. Indeed the seasonal dependence and the percentage occurrence of H_S from January to December delineate their contribution to the annual wave statistics on the regional scale. A detailed trend analysis on segregated H_S is conducted for the selected sub-domains. Almost all sectors of the IO, specifically the SIO revealed a declining trend of H_S during the 2007–2011 pentad and that coincides with the recorded two strong La Niña events. However, the IO wave climate is rather influenced by the combined Indian Ocean Dipole (IOD) events in which El Niño/La Niña are accompanied. In general it is observed that the mean wave trend of the TSIO follows that of the ETSI. During the last pentad 2012–2016, the trend of higher percentile H_S is noticed to increase over the AS, BoB, TSIO, ESTI, and the highest mean H_S recorded in 2016 corresponds to the strong El Niño event co-existent with a negative IOD event. It is inferred that the ENSO associated with the negative IOD resulted in an increased wave height. There is a dominant pentad cycle observed during 1997 and 2016 in the west and east of the ETSI in which the western sector exhibits the highest variability in all time, though the eastern side is observed with comparatively higher wave height. At the same time, the NIO and the TSIO are noticed with a decadal cycle at lower percentile wave heights.

References

Aboobacker VM, Shanas PR (2018a) The climatology of shamals in the Arabian Sea—Part 1: surface winds. Int J Climatol. https://doi.org/10.1002/joc.5711

Aboobacker VM, Shanas PR (2018b) The climatology of shamals in the Arabian Sea—Part 2: surface waves. Int J Climatol. https://doi.org/10.1002/joc.5677

Aboobacker VM, Vethamony P, Rashmi R (2011) "Shamal" swells in the Arabian Sea and their influence along the west coast of India. Geophys Res Lett. https://doi.org/10.1029/2010GL045736

Alves JHGM (2006) Numerical modeling of ocean swell contributions to the global wind-wave climate. Ocean Model. https://doi.org/10.1016/j.ocemod.2004.11.007

Amrutha MM, Sanil Kumar V, Sandhya KG, Balakrishnan Nair TM, Rathod JL (2016) Wave hindcast studies using SWAN nested in WAVEWATCH III—comparison with measured nearshore buoy data off Karwar, eastern Arabian Sea. Ocean Eng. https://doi.org/10.1016/j.oceaneng.2016.04.032

Anoop TR, Sanil Kumar V, Shanas PR, Johnson G (2015) Surface wave climatology and its variability in the north Indian Ocean Based on ERA-interim reanalysis. J Atmos Ocean Technol. https://doi.org/10.1175/JTECH-D-14-00212.1

Anoop TR, Sanil Kumar V, Shanas PR, Glejin J, Amrutha MM (2016) Indian Ocean Dipole modulated wave climate of eastern Arabian Sea. Ocean Sci 12:369–378

Anoop TR, Shanas PR, Aboobacker VM, Sanil Kumar V, Sheela Nair L, Prasad R, Reji S (2020) On the generation and propagation of Makran swells in the Arabian Sea. Int J Climatol 40(1):585–593. https://doi.org/10.1002/joc.6192

Arora K, Dash P (2019) The Indian ocean dipole: a missing link between El Niño Modokiand tropical cyclone intensity in the North Indian ocean. Climate 7:3. https://doi.org/10.3390/cli7030038

Bhaskaran PK (2014) Wind-wave climate projections for the Indian Ocean from satellite observations. J Mar Sci Res Dev. https://doi.org/10.4172/2155-9910.s11-005

Bhaskaran PK (2019) Challenges and future directions in ocean wave modeling—a review. J Extreme Events. https://doi.org/10.1142/s2345737619500040

Cavaleri L (2000) The oceanographic tower Acqua Alta—activity and prediction of sea states at Venice. Coast Eng 39:29–70. https://doi.org/10.1016/S0378-3839(99)00053-8

Cavaleri L, Bertotti L (2004) Accuracy of the modelled wind and wave fields in enclosed seas. Tellus A 56:167–175. https://doi.org/10.1111/j.1600-0870.2004.00042.x

Cavaleri L, Bertotti L, Buizza R, Buzzi A, Masato V, Umgiesser G, Zampieri M (2010) Predictability of extreme meteo-oceanographic events in the Adriatic Sea. Q J R Meteorol Soc 136:400–413. https://doi.org/10.1002/qj.567

Chandramohan P, Kumar V, Nayak B (1990) Wave statistics around the Indian coast based on ship observed data. Indian J Mar Sci 20:87–92

Galanis G, Kallos G, Dodson CTJ, Chu PC, Kuo Y-H (2012) Wave height characteristics in the north Atlantic ocean: a new approach based on statistical and geometrical techniques. Stoch Environ Res Risk Assess. https://doi.org/10.1007/s00477-011-0540-2

Gowthaman R, Sanil Kumar V, Dwarakish GS, Mohan SS, Singh J, Ashok Kumar K (2013) Waves in Gulf of Mannar and Palk Bay around Dhanushkodi, Tamil Nadu, India. Curr Sci 104(10):1431–1435

Gupta N, Bhaskaran PK, Dash MK (2015) Recent trends in wind-wave climate for the Indian Ocean. Curr Sci 108(12):2191–2201

Gupta N, Bhaskaran PK, Dash MK (2017) Dipole behaviour in maximum significant wave height over the Southern Indian Ocean. Int J Climatol. https://doi.org/10.1002/joc.5133

Hersbach H, Dick L (2016) ERA5 reanalysis is in production. ECMWF Newsl

Hoffmann L et al (2019) From ERA-interim to ERA5: the considerable impact of ECMWF's next-generation reanalysis on Lagrangian

transport simulations. Atmos Chem Phys. https://doi.org/10.5194/acp-19-3097-2019

Komen GJ, Cavaleri L, Donelan M, Hasselmann K, Hasselmann S, Janssen PAEM (1994) Dynamics and modelling of ocean waves. Cambridge University Press, Cambridge, p 532

Kumar VS, Naseef TM (2015) Performance of ERA-interim wave data in the nearshore waters around India. J Atmos Ocean Technol. https://doi.org/10.1175/JTECH-D-14-00153.1

Kumar ED, Sannasiraj SA, Sundar V, Polnikov VG (2013) Wind-wave characteristics and climate variability in the Indian Ocean Region using altimeter data. Mar Geodesy. https://doi.org/10.1080/01490419.2013.771718

Kumar P, Min S-K, Weller E, Lee H, Wang XL (2016) Influence of climate variability on extreme ocean surface wave heights assessed from ERA-interim and ERA-20C. J Clim. https://doi.org/10.1175/JCLI-D-15-0580.1

Kumar P, Kaur S, Weller E, Min S-K (2019) Influence of natural climate variability on the extreme ocean surface wave heights over the Indian Ocean. J Geophys Res Ocean 124(8):6176–6199

Kurian NP, Rajith K, Shahul Hameed TS, Sheela Nair L, Ramana Murthy MV, Arjun S, Shamji VR (2009) Wind waves and sediment transport regime off the south-central Kerala coast, India. Nat Hazards. https://doi.org/10.1007/s11069-008-9318-3

Lin G, Shao LT, Zheng CW, Chen XB, Zeng LF, Liu ZH, Li RB, Shi WL (2017) Assessment of wave energy in the South China sea based on GIS technology. Adv Meteorol. https://doi.org/10.1155/2017/1372578

Mahmood S, Davie J, Jermey P, Renshaw R, George JP, Rajagopal EN, Indira Rani S (2018) Indian monsoon data assimilation and analysis regional reanalysis: configuration and performance. Atmos Sci Lett. https://doi.org/10.1002/asl.808

Moorthi S, Pan H-L, Caplan P (2001) Changes to the 2001 NCEP operational MRF/AVN global analysis/forecast system. NWS Tech Procedures Bull 484:20

Muhammed Naseef T, Sanil Kumar V (2019) Climatology and trends of the Indian Ocean surface waves based on 39-year long ERA5 reanalysis data. Int J Climatol. https://doi.org/10.1002/joc.6251

Nayak S, Bhaskaran PK, Venkatesan R, Dasgupta S (2013) Modulation of local wind-waves at Kalpakkam from remote forcing effects of Southern Ocean swells. Ocean Eng. https://doi.org/10.1016/j.oceaneng.2013.02.010

Parsons MJ, Crosby AR, Orelup L, Ferguson M, Cox AT (2018) Evaluation of ERA5 reanalysis wind forcing for use in ocean response modeling. Waves in shallow environments (WISE) 2018, April 22–26, 2018, Tel Aviv University, Tel Aviv, Israel. https://www.oceanweather.com/about/papers/index.html

Patra A, Bhaskaran PK (2016) Trends in wind-wave climate over the head Bay of Bengal region. Int J Climatol. https://doi.org/10.1002/joc.4627

Patra A, Bhaskaran PK (2017) Temporal variability in wind-wave climate and its validation with ESSO-NIOT wave atlas for the head Bay of Bengal. Clim Dyn. https://doi.org/10.1007/s00382-016-3385-z

Pomaro A, Cavaleri L, Papa A, Lionello P (2018) Data descriptor: 39 years of directional wave recorded data and relative problems, climatological implications and use. Sci Data. https://doi.org/10.1038/sdata.2018.139

Queffeulou P (2003) Long-term quality status of wave height and wind speed measurements from satellite altimeters. In: Proceedings of the international offshore and polar engineering conference

Queffeulou P (2004) Long-term validation of wave height measurements from altimeters. Mar Geodesy. https://doi.org/10.1080/01490410490883478

Remya PG, Vishnu S, Praveen Kumar B, Balakrishnan Nair TM, Rohith B (2016) Teleconnection between the North Indian Ocean high swell events and meteorological conditions over

the Southern Indian Ocean. J Geophys Res Oceans. https://doi.org/10.1002/2016jc011723

Schott FA, McCreary JP (2001) The monsoon circulation of the Indian Ocean. Prog Oceanogr. https://doi.org/10.1016/S0079-6611(01)00083-0

Semedo A, Suselj K, Rutgersson A, Sterl A (2011) A global view on the wind sea and swell climate and variability from ERA-40. J Clim. https://doi.org/10.1175/2010JCLI3718.1

Shanas PR, Kumar VS (2015) Trends in surface wind speed and significant wave height as revealed by ERA-Interim wind wave hindcast in the Central Bay of Bengal. Int J Climatol. https://doi.org/10.1002/joc.4164

Shanas PR, Sanil Kumar V (2014a) Comparison of ERA-interim waves with buoy data in the eastern Arabian sea during high waves. Indian J Geo-Mar Sci 43(7):1343–1346

Shanas PR, Sanil Kumar V (2014b) Temporal variations in the wind and wave climate at a location in the eastern Arabian Sea based on ERA-Interim reanalysis data. Nat Hazards Earth Syst Sci. https://doi.org/10.5194/nhess-14-1371-2014

Shanas PR, Aboobacker VM, Albarakati AMA, Zubier KM (2017) Climate driven variability of wind-waves in the Red Sea. Ocean Model 119:105–117

Slingo J, Spencer H, Koskins B, Berrisford P, Black E (2005) The meteorology of the Western Indian Ocean, and the influence of the East African Highlands. Philos Trans R Soc A Math Phys Eng Sci. https://doi.org/10.1098/rsta.2004.1473

Stopa JE, Cheung KF (2014a) Intercomparison of wind and wave data from the ECMWF reanalysis interim and the NCEP climate forecast system reanalysis. Ocean Model. https://doi.org/10.1016/j.ocemod.2013.12.006

Stopa JE, Cheung KF (2014b) Periodicity and patterns of ocean wind and wave climate. J Geophys Res Ocean. https://doi.org/10.1002/2013jc009729

Stopa JE, Ardhuin F, Stutzmann E, Lecocq T (2019) Sea state trends and variability: consistency between models, altimeters, buoys, and seismic data (1979–2016). J Geophys Res Ocean. https://doi.org/10.1029/2018JC014607

Stow CA, Jolliff J, McGillicuddy DJ Jr, Doney SC, Icarus Allen J, Friedrichs MAM, Rose KA, Wallhead P (2009) Skill assessment for coupled biological/physical models of marine systems. J Mar Syst 76(1–2):4–15. https://doi.org/10.1016/j.jmarsys.2008.03.011

Swain J, Umesh P, Balchand A (2019) WAM and WAVEWATCH-III intercomparison studies in the North Indian Ocean using Oceansat-2 Scatterometer winds. J Ocean Clim Sci Technol Impacts. https://doi.org/10.1177/2516019219866569

Tolman HL (1991) A third-generation model for wind waves on slowly varying, unsteady, and inhomogeneous depths and currents. J Phys Oceanogr. https://doi.org/10.1175/1520-0485(1991)021%3c0782:atgmfw%3e2.0.co;2

Tolman HL (2009) User manual and system documentation of WAVEWATCH-IIITM version 3.14. Technical note. https://doi.org/10.3390/ijerph2006030011

van Sebille E, Sprintall J, Schwarzkopf FU, Sen Gupta A, Santoso A, England MH, Biastoch A, Boning CW (2014) Pacific-to-Indian ocean connectivity: Tasman leakage, Indonesian Throughflow, and the role of ENSO. J Geophys Res Oceans. https://doi.org/10.1002/2013jc009525

Vethamony P, Rao LVG, Kumar R, Sarkar A, Mohan M, Sudheesh K, Karthikeyan SB (2000) Wave climatology of the Indian Ocean derived from altimetry and wave model. In: Proceedings of PORSEC, Goa, India, pp 301–304

Vinoth J, Young IR (2011) Global estimates of extreme wind speed and wave height. J Clim 24:1647–1665

Young IR, Ribal A (2019) Multiplatform evaluation of global trends in wind speed and wave height. Science 364(6440):548–552. https://doi.org/10.1126/science.aav9527

Young IR, Zieger S, Babanin AV (2011) Global trends in wind speed and wave height. Science. https://doi.org/10.1126/science.1197219

Young IR, Vinoth J, Zieger S, Babanin AV (2012) Investigation of trends in extreme value wave height and wind speed. J Geophys Res Oceans. https://doi.org/10.1029/2011jc007753

Zheng CW, Pan J, Li CY (2016a) Global oceanic wind speed trends. Ocean Coast Manag. https://doi.org/10.1016/j.ocecoaman.2016.05.001

Zheng K, Sun J, Guan C, Shao W (2016b) Analysis of the global swell and wind sea energy distribution using WAVEWATCH III. Adv Meteorol. https://doi.org/10.1155/2016/8419580

Zheng CW, Li CY, Pan J (2018) Propagation route and speed of Swell in the Indian Ocean. J Geophys Res Oceans. https://doi.org/10.1002/2016jc012585